Impaired Cyclic Electron Flow around Photosystem I Disturbs High-Light Respiratory Metabolism[1]

Igor Florez-Sarasa[2], Ko Noguchi[2], Wagner L. Araújo, Ana Garcia-Nogales, Alisdair R. Fernie, Jaume Flexas, and Miquel Ribas-Carbo*

Max-Planck-Institut für Molekulare Pflanzenphysiologie, 14476 Potsdam-Golm, Germany (I.F.-S., A.R.F.); School of Life Sciences, Tokyo University of Pharmacy and Life Sciences, Hachioji, Tokyo 192-0392, Japan (K.N.); Max-Planck Partner Group at the Departamento de Biologia Vegetal, Universidade Federal de Viçosa, Vicosa, Minas Gerais 36570-000, Brazil (W.L.A.); Área de Ecología, Departamento Sistemas Físicos, Químicos y Naturales, Universidad Pablo de Olavide, 41013 Seville, Spain (A.G.-N.); and Grup de Recerca en Biologia de les Plantes en Condicions Mediterranies, Departament de Biologia, Universitat de les Illes Balears, 07122 Palma de Mallorca, Spain (J.F., M.R.-C.)

ORCID IDs: 0000-0002-1862-7931 (I.F.-S.); 0000-0002-6124-3415 (A.G.-N.); 0000-0002-7337-2089 (M.R.-C.).

The cyclic electron flow around photosystem I (CEF-PSI) increases ATP/NADPH production in the chloroplast, acting as an energy balance mechanism. Higher export of reducing power from the chloroplast in CEF-PSI mutants has been correlated with higher mitochondrial alternative oxidase (AOX) capacity and protein amount under high-light (HL) conditions. However, in vivo measurements of AOX activity are still required to confirm the exact role of AOX in dissipating the excess of reductant power from the chloroplast. Here, CEF-PSI single and double mutants were exposed to short-term HL conditions in Arabidopsis (*Arabidopsis thaliana*). Chlorophyll fluorescence, in vivo activities of the cytochrome oxidase (ν_{cyt}) and AOX (ν_{alt}) pathways, levels of mitochondrial proteins, metabolite profiles, and pyridine nucleotide levels were determined under normal growth and HL conditions. ν_{alt} was not increased in CEF-PSI mutants, while AOX capacity was positively correlated with photoinhibition, probably due to a reactive oxygen species-induced increase of AOX protein. The severe metabolic impairment observed in CEF-PSI mutants, as indicated by the increase in photoinhibition and changes in the levels of stress-related metabolites, can explain their lack of ν_{alt} induction. By contrast, ν_{cyt} was positively correlated with photosynthetic performance. Correlations with metabolite changes suggest that ν_{cyt} is coordinated with sugar metabolism and stress-related amino acid synthesis. Furthermore, changes in glycine-serine and NADH-NAD^+ ratios were highly correlated to ν_{cyt}. Taken together, our results suggest that ν_{cyt} can act as a sink for the excess of electrons from the chloroplast, probably via photorespiratory glycine oxidation, thus improving photosynthetic performance when ν_{alt} is not induced under severe HL stress.

Respiration in leaf tissues is influenced by their photosynthetic metabolism, while respiratory metabolism affects photosynthesis. This forward-reverse interaction between photosynthesis and respiration has received a great deal of attention during the last decades (Krömer, 1995; Atkin et al., 2000; Raghavendra and Padmasree, 2003; Flexas et al., 2006; Yoshida and Noguchi, 2010; Araújo et al., 2014b; Obata et al., 2016). Essentially, while photosynthesis provides carbohydrates for glycolysis, mitochondrial metabolism in illuminated leaves supports photosynthesis, photorespiration, nitrogen metabolism, and the export of redox equivalents (Yoshida and Noguchi, 2010). Among different redox shuttles, the malate valve operates between chloroplasts, cytosol, and mitochondria (Scheibe, 2004), thus allowing the oxidation of chloroplast reductants by the mitochondrial electron transport chain (mETC; Yoshida and Noguchi, 2010). Particularly under high-light (HL) conditions, the alternative components of the mETC have been suggested to accomplish non-phosphorylating oxidation of the excess of reductants from the chloroplast (Yoshida and Noguchi, 2010).

The plant mETC is highly branched compared with mitochondria from other eukaryotic cells, given that it contains different alternative components that bypass the main complexes of the oxidative phosphorylation pathway: the cytochrome *c* oxidase (COX) pathway (Rasmusson et al., 2008). Among these energy-bypass

[1] This work was supported by the Spanish Ministry of Science and Innovation (project nos. BFU2008–1072/BFI and BFU2011–23294 to J.F., M.R.-C., and I.F.-S.), the Max Planck Society (to A.R.F. and W.L.A.), and the Alexander von Humboldt Foundation (to I.F.-S.).

[2] These authors contributed equally to the article.

* Address correspondence to mribas@uib.cat.

The author responsible for distribution of materials integral to the findings presented in this article in accordance with the policy described in the Instructions for Authors (www.plantphysiol.org) is: Miquel Ribas-Carbo (mribas@uib.cat).

I.F.-S., K.N., and M.R.-C. conceived the research plan and designed the experiments; I.F.-S. and K.N. performed all the respiration measurements; I.F.-S., K.N., and A.G.-N. performed all the photosynthesis measurements and sampling for protein and metabolic analyses; M.R.-C. and J.F. supervised the respiration and photosynthesis experiments and discussed the data; W.L.A. performed the GC-MS metabolite profiling analysis, and the data generated were analyzed by I.F.-S. together with A.R.F.; western-blot and pyridine nucleotide analyses were performed by I.F.-S.; I.F.-S. and K.N. wrote the article; A.R.F., J.F., and M.R.-C. assisted with the writing of the article; all authors read and approved the final article after critical revision.

www.plantphysiol.org/cgi/doi/10.1104/pp.16.01025

systems, the mETC is branched at the ubiquinone (UQ) pool from which the electrons of ubiquinol are used by alternative oxidase (AOX) to reduce oxygen to water without proton translocation (Moore and Siedow, 1991). In this way, AOX activity can bypass complex III and COX (complex IV), greatly reducing the efficiency of ATP synthesis by the mETC. More than two decades ago, it was shown that the AOX pathway competes with the COX pathway for the electrons of the UQ pool (Hoefnagel et al., 1995; Ribas-Carbo et al., 1995). These findings imply that the actual in vivo electron partitioning between the COX and AOX pathways can be determined by oxygen isotope fractionation during respiration but not using chemical inhibitors of the two pathways (Day et al., 1996; Ribas-Carbo et al., 2005). While several theories have been formulated about the role of AOX in plants (Gupta et al., 2009; Rasmusson et al., 2009; Van Aken et al., 2009; Vanlerberghe, 2013), there is still little confirmation of such roles by measuring AOX activity in vivo as determined by oxygen isotope fractionation (Yoshida and Noguchi, 2010; Vanlerberghe, 2013).

Transgenic approaches altering mitochondrial metabolism have provoked different effects on photosynthesis in plants with suppressed tricarboxylic acid cycle enzymes (for review, see Nunes-Nesi et al., 2011; Araújo et al., 2014b) or mETC components (Dutilleul et al., 2003; Sweetlove et al., 2006; Galle et al., 2010; Florez-Sarasa et al., 2011; Dahal et al., 2014). Genetic mutations in the main components of the respiratory chain such as complex I have drastic effects on photosynthesis and photorespiration (Dutilleul et al., 2003; Priault et al., 2006; Galle et al., 2010), and changes in the in vivo electron partitioning also were observed under drought stress and cell death (Vidal et al., 2007; Galle et al., 2010). With respect to the alternative components of the mETC, uncoupling protein (UCP) mutants in Arabidopsis (*Arabidopsis thaliana*) have shown altered photosynthesis due to a limitation in photorespiration (Sweetlove et al., 2006). Regarding AOX, an important role in optimizing photosynthesis has been reported in both Arabidopsis and tobacco (*Nicotiana tabacum*; Florez-Sarasa et al., 2011; Yoshida et al., 2011; Gandin et al., 2012; Dahal et al., 2014), including one study of AOX activity in vivo under HL conditions (Florez-Sarasa et al., 2011). Using AOX transgenic plants as an approach to determine its in vivo role, it has been confirmed that AOX is involved in preserving photosynthetic capacity under drought stress by reducing chloroplast overreduction and photodamage (Dahal et al., 2014, 2015).

As another approach to unravel the role of AOX in photosynthesis, respiratory properties have been examined in photosynthetic mutants, including the cyclic electron flow around PSI (CEF-PSI) mutants, and the FtsH2 metalloprotease required for the repair of damaged PSII (Yoshida et al., 2007, 2008). In the study of Yoshida et al. (2007), the authors reported a correlation between higher export of excess reductant power from the chloroplast with higher AOX capacity and protein amount in Arabidopsis mutants with altered CEF-PSI following HL treatment. These mutants showed higher AOX capacity and protein amount even under low-light conditions. Importantly, a general lack of relationship between the AOX protein content and its in vivo activity has been reported in HL stress experiments using Arabidopsis plants (Florez-Sarasa et al., 2011). Therefore, AOX in vivo activity measurements are crucial for elucidating the possible role of AOX in dissipating the excess of reductant power from the chloroplast.

Since various primary metabolites are involved in interactions between chloroplasts and mitochondria, such as photorespiration and reductant transport, the levels of primary metabolites may be changed following deficiencies in photosynthesis or respiration and by environmental perturbations. We demonstrated previously that a large number of metabolites increased in leaves of Arabidopsis growing in or transiently exposed to HL conditions (Florez-Sarasa et al., 2012). The AOX1a deficiency in Arabidopsis altered the levels of certain metabolites, such as sugars and sugar phosphates, in the shoots under low-nitrogen stress (Watanabe et al., 2010). However, changes in primary metabolite levels have not yet been related to in vivo partitioning between COX and AOX pathways in photosynthetic (i.e. CEF-PSI) mutants.

Here, we investigated the effects of HL treatment on the in vivo activities of COX and AOX pathways in leaves of Arabidopsis mutants defective in CEF-PSI (Fig. 1). Our hypothesis is that CEF-PSI mutants will present higher in vivo flux through AOX to dissipate the excess of reducing power from the chloroplast under HL conditions. We also examined photosynthetic properties using chlorophyll fluorescence and determined mitochondrial proteins and primary metabolite levels in an attempt to clarify the underlying mechanisms regulating the in vivo activities of COX and AOX pathways under HL conditions.

RESULTS

Chlorophyll Fluorescence Parameters under Growth Light and after HL Treatment

Under growth light (GL) conditions, photochemical quenching (qP) and nonphotochemical quenching (qN and NPQ) were similar in wild-type *glabra1* (*gl1*) plants and single mutants (*pgr5* [for proton gradient reduction] and *crr4-3* [for chlororespiratory reduction]; Fig. 2). qN and NPQ also were unaltered in double mutants (*pgr5 crr4-3*) compared with the other lines (Fig. 2, B and D), while qP was clearly lower in this genotype (Fig. 2A). The quantum efficiency of PSII (ΦPSII) and the electron transport rate (ETR) were similar in *gl1*, *crr4-3*, and *pgr5*, while both were lower in the *pgr5 crr4-3* double mutants (Fig. 2, C and E). In addition, the maximum efficiency of PSII (F_v/F_m) also was lower in double mutants compared with the other three lines (Fig. 2F) and, in agreement, the percentages of total photoinhibition (%TPI) and chronic photoinhibition (%CPI) in the double mutants were significantly higher than in the other lines (Table I).

Under HL conditions, qP was decreased similarly in all lines, while NPQ and qN were increased (Fig. 2, A, B,

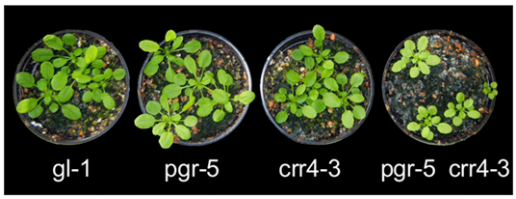

Figure 1. Photograph of representative wild-type (*gl1*) and CEF-PSI mutant plants after 4 weeks of growth. The light treatments, measurements, and harvesting were performed after 4 weeks of growth in *gl1* and CEF-PSI single mutant plants (*crr4-3* and *pgr5*), which showed slight growth retardation. On the other hand, double mutants (*pgr5 crr4-3*) presented pale green leaves and a more pronounced growth retardation; therefore, they were grown for 5 weeks to reach a similar developmental stage to the other genotypes.

and D). During HL treatment, qN was decreased significantly only in double mutants (Fig. 2, B and D). NPQ was slightly but significantly reduced in *pgr5* and *crr4-3* at 8 h of HL treatment, while it was much more reduced in double mutants already at 4 h of HL treatment (Fig. 2, B and D). ΦPSII and electron transport rate (ETR) generally were lower in both *pgr5* and double mutants compared with *gl1* and *crr4-3* (Fig. 2, C and E). The ETR in both *gl1* and *crr4-3* increased after 2 h of HL treatment and then decreased afterward; this initial increase was lacking in *pgr5* and double mutant plants (Fig. 2E). On the other hand, F_v/F_m was decreased in all lines after HL treatment (Fig. 2F). However, while F_v/F_m displayed a similar decrease in *gl1* and *crr4-3*, it was more reduced in *pgr5* and the double mutant, the latter showing the lowest values after HL treatment (Fig. 2F). Finally, %TPI was significantly higher in *pgr5* and double mutants than in *gl1* and *crr4-3*, mainly due to higher % CPI (Table I). Among all the genotypes, double mutants exhibited the highest values of %TPI and %CPI (Table I). Following the HL induction, %CPI was kept constant in all genotypes with the exception of the double mutants, in which it was increased further at 4 h of HL treatment (Table I). Finally, the percentage of dynamic photoinhibition (%DPI) presented a similar pattern to that of qN and NPQ in all genotypes. Thus, %DPI was increased and kept high during the HL treatment in *gl1* and *crr4-3* plants, whereas it was increased further in *pgr5* and double mutants after 2 h of HL treatment but then decreased at 4 and 8 h of HL treatment (Table I).

In Vivo Activities of the COX and AOX Pathways under GL and after HL Treatment

The rates of respiration in Figure 3 are presented on a dry weight basis due to the differences in the specific leaf weight (leaf dry weight per area) observed between lines (data not shown). Under GL conditions, V_t as well as ν_{cyt} and ν_{alt} were similar in all four genotypes (Fig. 3). However, V_{alt}, which is a proxy for the AOX protein content, was 2-fold higher in double mutants compared with the other lines (Fig. 3D).

Under HL conditions, V_t increased significantly in all genotypes, peaking at 2 h, and then decreased toward 8 h after HL stress. However, the *pgr5* and double mutants presented a lower HL induction of V_t than *gl1* and *crr4-3* plants (Fig. 3A). Notably, the double mutants were the least responsive genotype, reaching similar V_t rates at 8 h as in GL conditions (Fig. 3A). The pattern of HL induction of ν_{cyt} was similar to that of V_t (Fig. 3B). On the other hand, ν_{alt} was almost unchanged in all lines, with the exception of a significant increase only in *gl1* after 2 h of HL treatment (Fig. 3C). However, V_{alt} exhibited a general induction pattern with the exception of the *crr4-3* plants, which kept constant rates until 8 h of HL treatment. V_{alt} was increased significantly only in *pgr5* (1.5-fold increase) and double mutants (1.3-fold increase) after 4 and 8 h of HL treatment (Fig. 3D), with the double mutants always exhibiting the highest V_{alt} (Fig. 3D).

Relationships between Photosynthetic Parameters and in Vivo Respiratory Activities after HL Treatment

The photosynthetic parameters obtained from chlorophyll fluorescence measurements were correlated to the respiratory parameters determined by oxygen isotope fractionation during respiration across genotypes under HL conditions (Table II; Supplemental Fig. S1). V_t was positively and significantly correlated with the ETR, qN, NPQ, and F_v/F_m, indicating both a direct link between respiration and photosynthetic electron transport chain activity as well as its degree of photoinhibition under HL conditions. Indeed, the %TPI was negatively and significantly correlated to V_t, with the %CPI being the main contributor to the negative correlation to photoinhibition. It was clearly observed that ν_{cyt}, but not ν_{alt}, was linked to the chloroplast electron transport chain activity and its degree of photoinhibition under HL conditions (Table II). On the other hand, almost all of the photosynthetic parameters correlated significantly with V_{alt}. Notably, the correlations of the photosynthetic parameters with V_{alt} were in the opposite direction to those observed with V_t and ν_{cyt}, thus being negative to photosynthetic activity (i.e. ETR) and positive to photoinhibition (%TPI and %CPI).

mETC Protein Levels under GL and after HL Treatment

Different mETC proteins were immunodetected by western-blot analyses in whole leaf extracts, including AOX, COX subunit II (COXII), and UCP. In addition, porin levels also were determined as a control for mitochondrial protein loading and remain similar in all the genotypes and light conditions (Fig. 4; Supplemental Fig. S2). Band intensities were quantified for all the proteins, and AOX, COXII, and UCP levels were obtained after correction by the corresponding porin band intensities and then normalized to the levels of the *gl1* plants under GL (i.e. *gl1* levels for all the proteins are 100%). Two independent experiments were performed (for details,

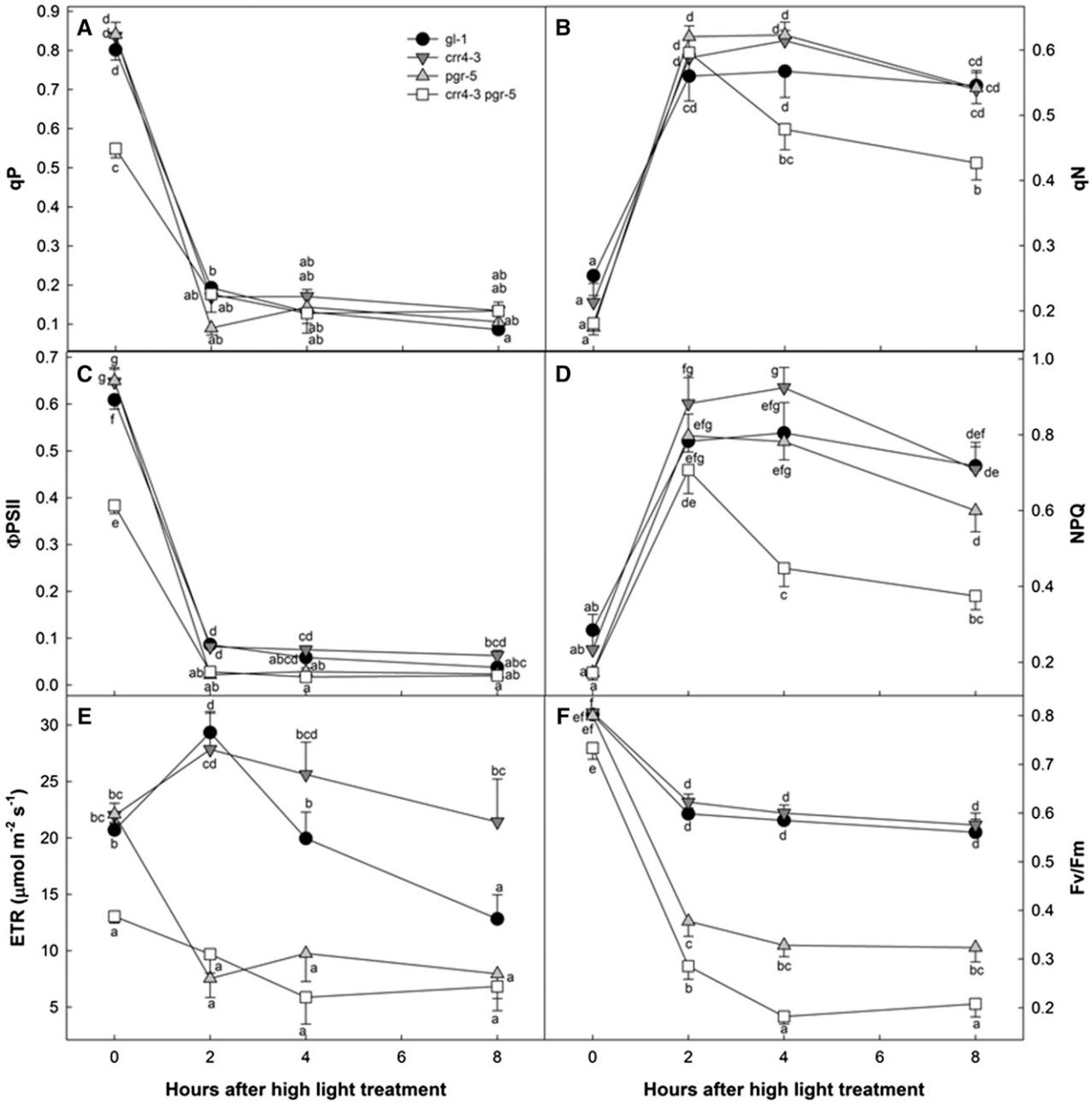

Figure 2. Photosynthetic parameters obtained by chlorophyll fluorescence analysis in the wild type (*gl1*) and CEF-PSI mutants. qP (A), qN (B), ΦPSII (C), NPQ (D), chloroplast ETR (E), and F_v/F_m (F) were determined in leaves of *gl1*, *crr4-3*, *pgr5*, and *pgr5 crr4-3* plants under GL (0 h) and after 2, 4, and 8 h of HL treatment. The chlorophyll fluorescence analyses, parameter calculations, light treatments, and genotypes are detailed in "Materials and Methods." Data represent means ± SE of 10 to 12 replicates, and different letters denote statistically significant differences ($P < 0.05$).

see "Materials and Methods"), and the average of the two relative quantifications is presented together with the image of the most representative blot (Fig. 4). The levels of AOX protein were approximately 2-fold higher in double mutants than in the other genotypes under GL conditions (Fig. 4), which coincides with the highest AOX capacity observed in these plants (Fig. 3D). By contrast, COX protein levels were lower in the double mutants, and UCP levels were similar in all genotypes (Fig. 4). Following HL treatment, the levels of UCP and COX remain relatively constant in all the genotypes compared with their respective levels under GL, with the exception of COX decreases observed after 8 h of HL treatment in *gl1* and *crr4-3* plants (Fig. 4). On the other hand, the levels of AOX protein were increased in all genotypes after HL treatment, with *crr4-3* presenting the

Table I. *%TPI, %CPI, and %DPI in leaves of gl1, crr4-3, pgr5, and pgr5 crr4-3 plants under GL and after 2, 4, and 8 h of HL treatment*

%TPI, %CPI, and %DPI were obtained as described previously by Florez-Sarasa et al. (2011), and the F_v/F_{mmax} value was obtained from the mean value of F_v/F_{m30} under GL for *gl1* plants (i.e. %CPI in *gl1* plants is 0). Values are means ± SE of 10 to 12 replicates. Different letters denote significant differences ($P < 0.05$) between species.

Genotype	%TPI				%CPI				%DPI			
	GL	2 h HL	4 h HL	8 h HL	GL	2 h HL	4 h HL	8 h HL	GL	2 h HL	4 h HL	8 h HL
gl1	2.3 ± 0.5 a	38.5 ± 1.9 c,d	40.2 ± 2.7 c,d	41.7 ± 3.9 d	0.0 ± 0.3 a	26.4 ± 1.4 c,d	27.1 ± 2.3 c,d	30.1 ± 3.3 d	2.3 ± 0.2 a	12.1 ± 1.1d e	13.1 ± 0.8 d,e,f	11.6 ± 2.6 d,e
crr4-3	2.9 ± 0.4 a	32.8 ± 2.7 c	38.1 ± 2.7 c,d	38.7 ± 3.4 c,d	0.4 ± 0.4 a	20.9 ± 2.0 c	25.2 ± 2.1 c,d	28.3 ± 3.0 c,d	3.3 ± 0.2 a	11.9 ± 0.8 d,e	12.9 ± 0.9 d,e,f	10.5 ± 1.0 c,d,e
pgr5	3.4 ± 0.7 a	67.3 ± 3.4 e	68.8 ± 2.4 e	67.1 ± 3.7 e	0.3 ± 0.4 a	52.9 ± 3.9 e	59.1 ± 2.9 e,f	59.6 ± 3.7 e,f	3.0 ± 0.4 a	14.4 ± 1.0 e,f	9.7 ± 1.2 c,d	7.5 ± 0.8 b,c
pgr5 crr4-3	14.4 ± 3.9 b	81.1 ± 2.2 f	83.0 ± 1.2 f	79.8 ± 2.4 f	8.6 ± 2.8 b	64.4 ± 3.4 f	77.3 ± 2.0 g	74.1 ± 3.4 g	5.9 ± 1.1 a,b	16.7 ± 1.9 f	5.7 ± 1.6 a,b	5.7 ± 1.8 a,b

lowest increases. After 8 h of HL treatment, *pgr5* and double mutants presented the highest AOX levels (i.e. an approximately 3-fold increase; Fig. 4).

Metabolite Profiling and Pyridine Nucleotide Levels under GL and after HL Treatment

A total of 49 metabolites were identified using gas chromatography-mass spectrometry (GC-MS), including several amino acids, organic acids, some sugars, and sugar alcohols (Fig. 5; Supplemental Table S1). Mutant plants displayed significant differences in the relative levels of some metabolites under GL conditions compared with wild-type (*gl1*) plants (Fig. 5; Supplemental Table S1). In all mutant lines, the levels of Asp, Glu, and malate were significantly lower compared with *gl1* plants, while glycerate was significantly higher. In *pgr5* plants, the levels of Arg, Ser, γ-aminobutyrate, fumarate, 2-oxobutyrate, and shikimate were significantly lower than in *gl1*. On the other hand, the levels of β-Ala, Gly, Orn, spermidine, Ser, Trp, Glc, and glyceraldehyde-3-phosphate were significantly higher in *crr4-3* than in *gl1* plants, while the levels of Arg, Asn, Thr, 2-oxoglutarate, shikimate, and myoinositol were lower. Finally, the double mutants displayed higher levels of β-Ala, Ile, Phe, 4-Hyp, Ser, Trp, Tyr, citrate, isocitrate, dehydroascorbate, galactonate, and lactate. Among the above-mentioned metabolites significantly affected in all the mutant plants, only a few metabolites were changed by more than 2-fold. Asn and Glu were 0.5- and 0.4-fold lower in *crr4-3*, whereas glycerate and Gly were 2.5- and 3.3-fold higher in *gl1*, respectively. Tyr and Trp levels were 2.3- and 8.4-fold higher in double mutants than in *gl1*.

After HL treatment, most of the metabolites were increased except for some organic acids showing significant decreases, such as ascorbate, glycerate, and shikimate (Fig. 5; Supplemental Table S1). Some metabolites displayed dynamic responses over time after HL treatment (i.e. first increased and then decreased or vice versa), such as mannitol, Glc, Gal, succinate, shikimate, and Lys. Nevertheless, several metabolites presented a genotype-specific response to the HL treatment, such as Gly and ascorbate among others. These metabolite changes are described below according to their compound class.

Amino acids showed the highest increases after HL treatment, with the exception of Cys, γ-aminobutyrate, Gln, Ile, Leu, and putrescine, which remained largely unchanged. Gly was the metabolite exhibiting the highest HL induction, being increase approximately 13-fold in *gl1* and *crr4-3* at 8 h of HL treatment. However, Gly levels were increased approximately 5-fold in the *pgr5* mutant and were increased marginally by less than 2-fold in the double mutants after HL treatment. Pro was the second most induced metabolite under HL treatment, being increased progressively and similarly in all genotypes until 8 h of HL treatment. Tyr levels increased after HL treatment in all genotypes, and notably, double mutants showed the highest levels after 8 h of HL treatment (approximately 10-fold). Several

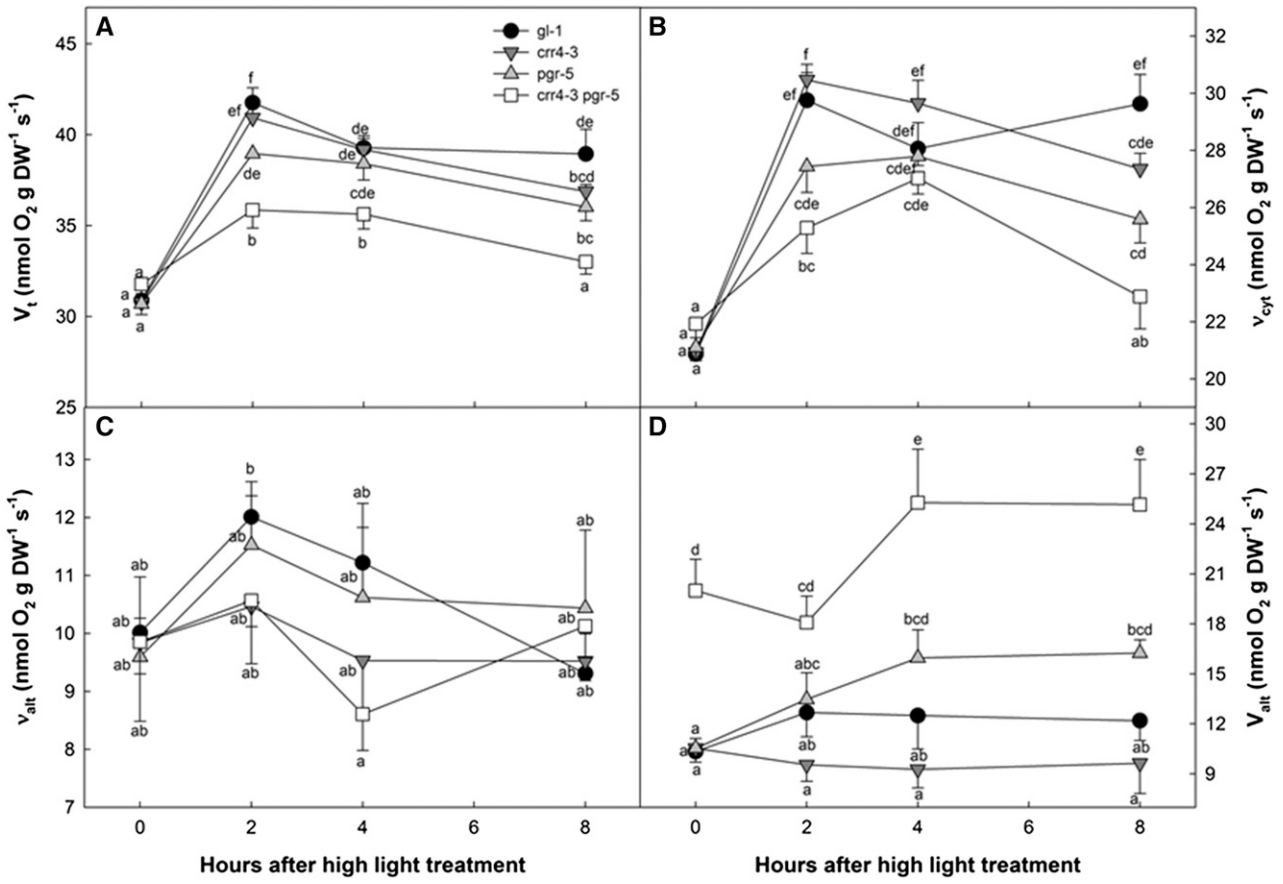

Figure 3. In vivo respiratory activities and capacity of the AOX in the wild type (*gl1*) and CEF-PSI mutants. Total respiration (V_t; A), COX pathway activity in vivo (v_{cyt}; B), AOX pathway activity in vivo (v_{alt}; C), and AOX capacity (V_{alt}; D) were determined in leaves of *gl1*, *crr4-3*, *pgr5*, and *pgr5 crr4-3* plants under GL (0 h) and after 2, 4, and 8 h of HL treatment. The respiration analyses, light treatments, and genotypes are detailed in "Materials and Methods." Data represent means ± SE of four to 10 replicates, and different letters denote statistically significant differences ($P < 0.05$). DW, Dry weight.

other amino acids showed about 2-fold increases after HL treatment. Ala, β-Ala, and Thr were increased significantly and continuously after HL treatment in all genotypes. Arg, homoserine, and Met also were increased significantly in all genotypes, but to a lesser extent in *pgr5* and double mutants, after 8 h of HL treatment. Glu was increased significantly in all genotypes, but to a lesser extent in *gl1*; Asp showed a similar although less pronounced response to Glu. Val was increased after 2 h of HL treatment and then maintained at high levels in all genotypes. A similar trend was observed in the Phe HL response in general, although *pgr5* and double mutants presented lower increases. Lys levels increased after 2 h of HL treatment and decreased subsequently; this pattern was observed in all genotypes, although the induction was less pronounced in the double mutants. Asn displayed a similar pattern to Lys except in *gl1* plants. Finally, 4-Hyp, Ser, spermidine, and Trp levels increased significantly after HL treatment in all genotypes, but generally by less than 2-fold. Orn level increased significantly after 8 h of HL treatment only in *gl1* and *crr4-3* lines.

In contrast to the HL-induced changes in amino acid levels, organic acids displayed some significantly and pronounced decreases, whereas increases of this compound class were few. For instance, malate and 2-oxoglutarate levels were increased continuously after HL treatment in all

Table II. *Pearson correlation coefficients between photosynthetic and respiratory parameters*

Twelve data points, corresponding to the means for each parameter of each genotype under the different hours of HL treatment, were used in the correlation analyses. Values in boldface indicate statistically significant Pearson correlations ($P < 0.05$).

Parameter	V_t	v_{cyt}	v_{alt}	V_{alt}
ETR	**0.74**	**0.73**	0.25	**−0.75**
F_v/F_m	**0.80**	**0.81**	0.22	**−0.92**
qP	0.29	0.22	0.24	−0.14
NPQ	**0.85**	**0.78**	0.39	**−0.89**
qN	**0.66**	0.56	0.41	**−0.69**
%TPI	**−0.76**	**−0.80**	−0.14	**0.88**
%CPI	**−0.80**	**−0.81**	−0.21	**0.92**
%DPI	0.53	0.39	0.47	**−0.60**

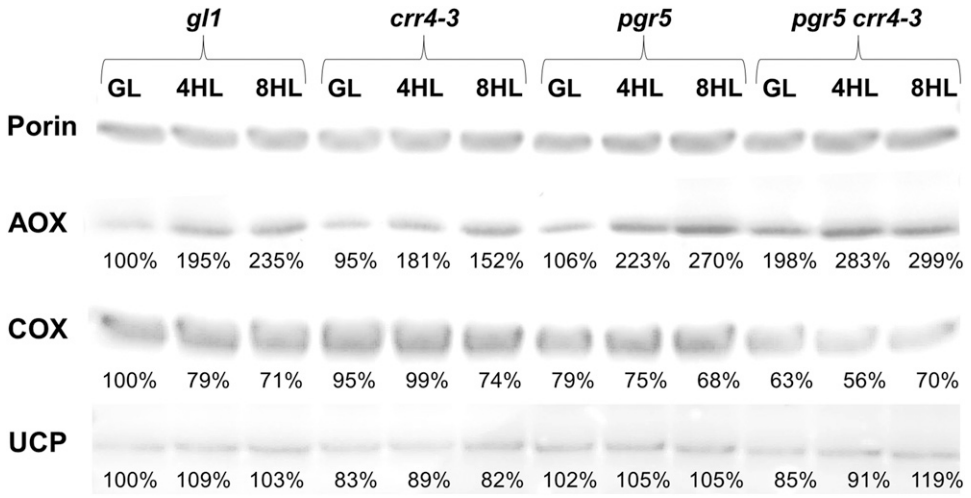

Figure 4. mETC proteins detected by western blot in leaves of *gl1*, *crr4-3*, *pgr5*, and *pgr5 crr4-3* plants under GL and after 4 and 8 h of HL treatment. The intensities of the signals from AOX, COXII, and UCP were normalized to those from porin and are expressed as percentages relative to values of *gl1* under GL intensity. The percentage values denoted are averages of two independent blots each using two biological replicates.

genotypes, although the response of 2-oxoglutarate was less pronounced in *pgr5* and double mutants. Similarly, dehydroascorbate increased over time in all genotypes, but the response was much lower in the double mutants. Also, citrate and fumarate levels presented slight but significant increases after HL treatment in all lines, and the levels in the double mutants again displayed a milder increase, if any. Succinate levels increased after 2 h and then decreased toward 8 h of HL treatment; this pattern was observed in all genotypes, but the induction was less pronounced in the double mutants. An inverse pattern was observed for shikimate, for which the levels decreased at 2 h after HL treatment in all genotypes but then increased at 4 and 8 h after HL treatment. The ascorbate level was decreased greatly and continuously in *gl1* and *crr4-3* following HL treatment. In *pgr5* mutants, significant decreases in ascorbate were observed only after 4 and 8 h, while a significant decrease was observed in double mutants only after 8 h of HL treatment. Glycerate also decreased significantly to similar levels in all genotypes after HL treatment, although the levels in *crr4-3* were much higher under GL conditions. As reported above, the levels of galactonate, isocitrate, and lactate were significantly higher in the double mutants in all conditions, and these metabolites generally were not altered after HL treatment. Pyruvate levels remained mostly unchanged after HL treatment in all the lines, and the same was observed for 2-oxobutyrate and benzoate, except for slight increases in the double mutant after 8 h of HL treatment.

With respect to the sugars and sugar alcohols, Gal, Glc, and mannitol levels peaked after 2 h and then decrease toward 8 h of HL treatment in all genotypes, and again, double mutants displayed a lower HL response. Erythritol also was increased, although to a lesser extent and mostly at the end of the HL treatment in all genotypes. A minor increase also was observed in glyceraldehyde-3-phosphate levels, but it was apparent only in *gl1* plants. On the other hand, Fru and Suc were not altered after HL treatment in any genotype, and myoinositol generally was lower in *crr4-3*.

In addition to single metabolite levels, relevant redox-related ratios were calculated (for details, see "Materials and Methods") and their HL response was compared among genotypes. The Gly-Ser ratio increased over time, reaching 9- and 10-fold increases at 8 h of HL treatment in *gl1* and *crr4-3*, respectively, while *pgr5* showed a reduced response (i.e. reaching a maximum of 4-fold increase). More severely dampened, double mutants exhibited a lack of HL induction on Gly-Ser ratio. The malate-Asp ratio was increased after HL treatment in all the genotypes, mostly after 8 h of HL treatment. The Glu-2-oxoglutarate ratio was much higher in *gl1* under GL conditions compared with the other genotypes. The Glu-2-oxoglutarate ratio decreased after 2 h of HL treatment in *gl1* and *crr4-3* but not in *pgr5* and double mutants. Finally, the 2-oxuglutarate-citrate ratio generally showed increases after HL treatment in all genotypes but were less pronounced in *pgr5* and double mutants.

In order to further investigate the redox changes in the CEF-PSI mutants, we measured the levels of NAD^+, NADH, $NADP^+$, and NADPH and calculated the corresponding redox ratios (Supplemental Fig. S3) in leaf samples of all genotypes and light conditions. Generally, no statistical differences in pyridine nucleotide levels were observed among genotypes when compared in each light condition. Nonetheless, some trends were observed after HL treatment: the levels of NAD^+ and NADH tended to increase in all genotypes after HL treatment (Supplemental Fig. S3). After 8 h of HL treatment, *gl1* showed the highest levels of NAD^+ compared with all other genotypes and conditions, while double mutants displayed the highest levels of NADH. As for NADH, the highest levels of NADPH we detected in double mutants after 8 h of HL treatment. With regard to the redox-related ratios, *gl1* plants generally displayed the lowest NADH-NAD^+ and NADPH-$NADP^+$ ratios, while double mutants displayed the highest ratios (Supplemental Fig. S3).

Relationships between Metabolite Levels and Respiratory Activities after HL Treatment

In order to obtain insights into the metabolic regulation or metabolic processes involved in the different

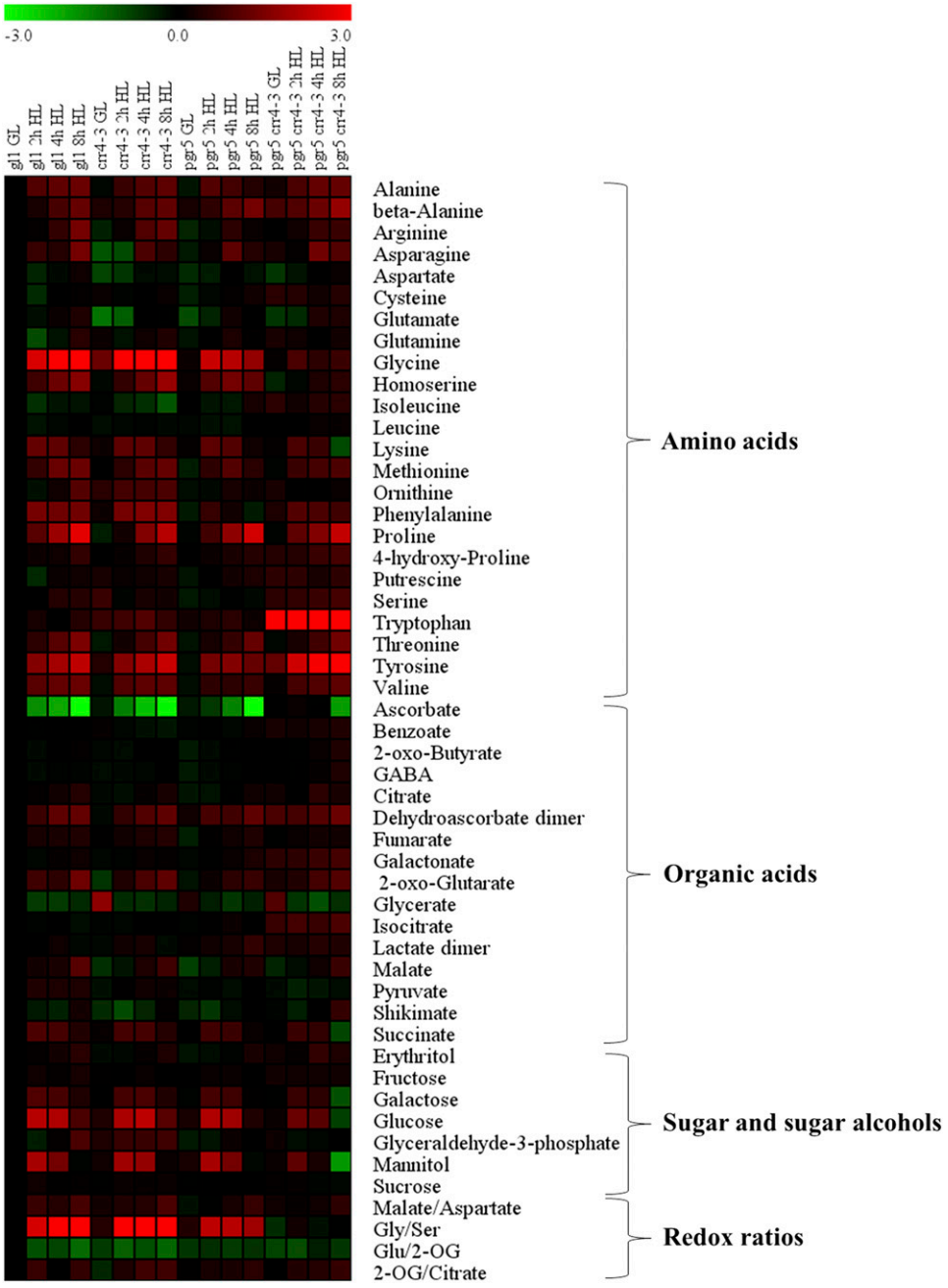

Figure 5. Heat map of the relative levels of the GC-MS-analyzed metabolites in the wild type (*gl1*) and CEF-PSI mutants under GL and after HL treatment. Metabolites were clustered per class into amino acids, organic acids, and sugars and sugar alcohols, and some metabolite ratios also were calculated. Relative metabolite levels in leaves of *gl1*, *crr4-3*, *pgr5*, and *pgr5 crr4-3* plants under all light conditions (for details, see "Materials and Methods") were normalized to the mean level of the *gl1* plants under GL conditions, and then fold change values were $\log_2$ transformed (i.e. the level of all metabolites of *gl1* plants under GL is 0). In this heat map, red and green colors represent $\log_2$ fold increased and decreased metabolites, respectively. Values are means ± SE of six replicates, and statistically significant differences from *gl1* plants under GL conditions are presented in Supplemental Table S1.

respiratory responses to HL treatment observed in the CEF-PSI mutants, Pearson correlation coefficients were calculated between the fold changes of metabolite levels and those of respiratory activity parameters across all four genotypes. Respiratory data were normalized to the mean of *gl1* plants under GL conditions, as was done for the relative metabolite level calculations, thus allowing 15 point correlations using the means for each genotype and light treatment. Positive (red) and negative (blue) significance values ($P < 0.05$) of the Pearson coefficients are shown in Figure 6. All correlation plots derived from significant ($P < 0.05$) correlations are shown in Supplemental Figure S4.

Changes in several amino acids, as affected by the genotype and the HL treatment, correlated positively and significantly with changes in V_t rates, including Gly, Lys, Ala, Phe, homoserine, Met, and Val. Only Ile changes were negatively correlated to V_t. Regarding organic acids, tricarboxylic acid cycle intermediates such as fumarate, 2-oxoglutarate, succinate, and pyruvate also were positively correlated to V_t, while glycerate was negatively correlated to it. On the other hand, sugars such as Glc, Gal, Suc, and the sugar alcohol mannitol were positively correlated to V_t. With regard to redox ratios, Gly-Ser and to a lesser extent 2-oxoglutarate-citrate ratios were positively correlated

Amino acids	V_t	ν_{cyt}	ν_{alt}
Alanine	0.69	0.73	
Arginine		0.55	
Glutamine			-0.56
Glycine	0.79	0.80	
Homoserine	0.67	0.70	
Isoleucine	-0.61	-0.60	
Leucine			-0.61
Lysine	0.78	0.76	
Methionine	0.66	0.72	
Phenylalanine	0.68	0.72	
Threonine		0.51	
Valine	0.73	0.78	
Organic acids			
Ascorbate		-0.51	
Benzoate		-0.50	
Fumarate	0.65	0.71	
2-oxo-Glutarate	0.53	0.62	
Glycerate	-0.74	-0.76	
Malate		0.53	
Pyruvate	0.64	0.63	
Succinate	0.76	0.75	
Sugars and sugar alcohols			
Galactose	0.77	0.75	
Glucose	0.83	0.79	
Mannitol	0.66	0.59	0.51
Sucrose	0.65	0.61	
Redox ratios			
Gly/Ser	0.80	0.80	
2-OG/Citrate	0.64	0.71	
NADH/NAD$^+$	-0.73	-0.67	-0.51

Figure 6. Pearson correlation coefficients between fold changes in metabolite levels and in vivo respiratory activities in the wild type (*gl1*) and CEF-PSI mutants. As for the calculation of relative metabolite levels, respiratory activities also were normalized to those of the *gl1* plants under GL conditions. Then, all fold change values were $\log_{10}$ transformed and used for the Pearson correlations. The values used for the correlations were means of all the genotypes under each light condition, thus allowing 15-point correlation. Only the metabolites showing statistically significant ($P < 0.05$) Pearson correlation coefficients to at least one respiratory parameter are presented, and their positive (red) and negative (blue) *r* values are shown.

to V_t. In addition, only NADH-NAD$^+$ ratios were significantly and negatively correlated with in vivo respiratory activities.

Notably, most of the observed significant correlations to V_t were driven mainly by ν_{cyt}, which, in addition, showed positive correlations to Arg, Thr, and malate and negative correlations to ascorbate and benzoate. On the other hand, changes in ν_{alt} presented only a positive correlation to mannitol and negative correlations to Gln and Leu. Among all the correlations presented in Figure 6, Glc and the Gly-Ser ratio with V_t and ν_{cyt} showed the highest Pearson coefficients.

DISCUSSION

The HL Treatment Caused a Severe Stress Response in *pgr5* and Double Mutants

The photosynthetic response of the wild-type (*gl1*) and the *crr4-3* single mutant plants after the HL treatment was generally similar, while a severely impaired photosynthetic response was observed in *pgr5* and double mutants. The *pgr5* mutant is deficient in the ferredoxin (Fd)-dependent CEF-PSI pathway (Munekage et al., 2002), while *crr4-3* is deficient in the NAD(P)H dehydrogenase (NDH)-dependent pathway (Kotera et al., 2005). While the Fd-dependent CEF-PSI is thought to be the predominant pathway in C3 photosynthesis, the NDH complex may act as a safety valve that prevents overreduction of the stroma (Shikanai, 2007). Although ΦPSII and qP were greatly decreased in wild-type (*gl1*) plants and the *crr4-3* mutant after 2 h of HL treatment, both genotypes presented an enhanced ETR after 2 h of HL treatment that was decreased toward the end of the light treatment. The NPQ and qN values also were up-regulated after 2 h of HL treatment in all genotypes, and this up-regulation was maintained during the HL treatment except for the double mutant. In *prg5 crr4-3* in high light, both the linear electron flow and CEF-PSI were suppressed (Shikanai, 2007). Thus, the proton gradient across the thylakoid membrane may be more gradual in the double mutant and, thereby, the NPQ and qN values were decreased. This HL inhibition of photosynthetic activity was related to the high level of photoinhibition denoted by the low F_v/F_m levels (Fig. 2) and increasing levels of calculated photoinhibition (Table I). Indeed, the %TPI observed in the wild type (*gl1*) was higher, around 40% (Table I), compared with the previously reported %TPI (i.e. less than 30%) in Arabidopsis Columbia-0 (Col-0) plants under very similar HL conditions (Florez-Sarasa et al., 2011). We used Arabidopsis *gl1* that is deficient in leaf trichomes (Oppenheimer et al., 1991) and plants of different developmental stages. Since trichomes can attenuate strong light (Steyn et al., 2002), this may explain the severity of the stress response observed in this study. In particular, the *pgr5* and double mutant (*pgr5 crr4-3*) were characterized by a very high %CPI after the HL treatment (Table I). A high %CPI is associated with damage of the PSII (Osmond, 1994; Demmig-Adams et al., 2012), mostly due to increased reactive oxygen species (ROS) production at the chloroplast electron transport chain (Pintó-Marijuan and Munné-Bosch, 2014). In this respect, the observed decreases in ascorbate levels and increased dehydroascorbate levels after HL stress (Fig. 4) denote an important ROS-induced antioxidant response compared with the previously reported and minor HL-induced changes of these metabolites in Arabidopsis Col-0 plants (Florez-Sarasa et al., 2012). In addition, Pro accumulated at very high levels in all genotypes, particularly after 8 h (Fig. 4). Pro is involved in ROS

detoxification under many abiotic stresses (Szabados and Savouré, 2010); notably, 4-Hyp levels, a product of Pro oxidation, were higher in the double mutants than in the other genotypes. In addition, other stress-related metabolites such as β-Ala (Stiti et al., 2011) and Tyr (Yoo et al., 2013) were higher in the double mutants at GL and accumulated further after HL treatment compared with the other genotypes. Particularly, the most increased metabolite in double mutants was Trp, which is a precursor for the synthesis of secondary metabolites such as phytoalexins, glucosinolates, and alkaloids and also of the hormone auxin (Radwanski and Last, 1995; Zhao, 2012). The reduced growth, observed previously by Munekage et al. (2004) and Yamamoto et al. (2011), and the stress-related phenotype of the double mutants may be related to the Trp accumulation, although further research will be needed to unravel the nature of this metabolic alteration.

AOX Pathway Activity in Vivo Was Not Higher in CEF-PSI Mutants, Thus Partially Refuting the Initial Hypothesis

AOX is hypothesized to be activated in order to dissipate the excess of reducing equivalents under HL stress (Yoshida et al., 2007). Therefore, a higher ν_{alt} was expected in *pgr5* and double mutants due to an even higher excess of reductants in the chloroplast than in *gl1* and *crr4-3* plants. Surprisingly, ν_{alt} in the *pgr5* and double mutants was not changed significantly after HL treatment, while it was increased significantly in *gl1* plants after 2 h of HL stress, as reported previously in Arabidopsis Col-0 plants (Florez-Sarasa et al., 2011, 2012). By contrast, the AOX capacity was more HL induced in *pgr5* than in *gl1* plants, as reported previously (Yoshida et al., 2007). More importantly, double mutants presented the highest V_{alt} even under GL conditions, and it was also increased significantly after HL stress. Furthermore, V_{alt} presented the highest positive correlation to %CPI, while negative correlations with photosynthetic activity (i.e. ETR; Table II) were observed. These results suggest that the production of ROS associated with the high %CPI (Demmig-Adams et al., 2012) probably increased the ROS-mediated signal that induces AOX expression (Rhoads et al., 2006) and, as a consequence, its capacity. Indeed, the levels of AOX protein were higher in double mutants under GL conditions and were induced further after HL treatment (Fig. 4), thus following very similar patterns to V_{alt} (Fig. 3D). On the other hand, the slightly better photosynthetic performance (i.e. higher ETR and NPQ and lower %CPI), compared with *gl1*, observed in *crr4-3* mutants may partially explain their lack of V_{alt} response following HL treatment. However, the nature of the absence of such a response of V_{alt} in *crr4-3* remains unclear. That said, it appears reasonable to assume that the milder HL response of the AOX protein levels is the limiting factor of the V_{alt} and ν_{alt} responses in *crr4-3* mutants. The ROS-mediated signaling pathway that induces AOX expression is not fully understood yet (Li et al., 2013). Notably, AOX was induced mostly in green but not in white areas from leaves of yellow variegated mutants exposed to HL stress (Yoshida et al., 2008), thus indicating that chloroplast photooxidative stress influenced AOX protein synthesis. The AOX expression and capacity were previously well correlated in CEF-PSI mutants under HL stress (Yoshida et al., 2007), although this does not indicate the in vivo activity (Florez-Sarasa et al., 2011). In this respect, data presented in Figures 3 and 4 are in agreement with previous observations, thus confirming that the induction of both AOX capacity and protein levels is not always associated with an increase of in vivo AOX activity (i.e. as in the double mutants). Indeed, it has been demonstrated that AOX is inhibited by lipid peroxidation products (Winger et al., 2005), which are likely to be produced under the photooxidative stress conditions applied in this study.

In Vivo COX Instead of AOX Activity Mediated the Mitochondrial Response to Severe HL Stress and Was Highly Coordinated with Photosynthetic Performance

As mentioned above, ν_{alt} was not increased in double mutants under severe HL stress conditions, probably due to a ROS inactivation of the AOX. Moreover, ν_{alt} also decreased in *gl1* plants from its levels at 2 h toward 4 and 8 h of HL treatment (Fig. 3). On the other hand, ν_{cyt} was induced significantly in all lines after HL treatment (Fig. 3). The observed ν_{cyt} induction was not due to COX protein level modifications, since the levels of immunodetected COXII in all genotypes were either similar or lower in HL than in GL conditions; these results indicate that the COX protein level did not limit mETC activity and that increased flux through COP may lead to greater turnover of the COX protein. Moreover, ν_{cyt} but not ν_{alt} was significantly and positively correlated with photosynthetic activity (ETR) and NPQ (Table II; Supplemental Fig. S1). Increases in the linear electron flow of PSII induce a proton gradient across thylakoid membranes, which leads to an induction of NPQ (Shikanai, 2007). Also, ν_{cyt} was negatively correlated to %TPI and %CPI. Therefore, ν_{cyt} was correlated with a better photosynthetic performance under severe HL stress. While ATP provision by ν_{cyt} has been reported as an important role for mitochondrial metabolism in leaves under illumination, there is a high need for energy dissipation under HL conditions that can be accomplished by mitochondrial metabolism (Yoshida and Noguchi, 2010). In this respect, it has been proposed that the COX pathway also can allow an uncoupled electron transport under situations of chronic oxidative stress through the activation of the UCPs (Rasmusson et al., 2009). In this study, UCP levels were generally similar among genotypes, and no substantial changes were detected after HL treatment (Fig. 4). However, posttranslational activation of UCPs cannot be discarded. Indeed, UCP has been shown to be activated by lipid peroxidation

products (Vercesi et al., 2006), which would inhibit ν_{alt} but not ν_{cyt}, as observed in here.

In Vivo COX Activity Is Highly Coordinated with Photorespiratory and Amino Acid Metabolism

The active CEF-PSI in *gl1* plants after 2 h of HL treatment can diminish the excess of reducing power by balancing NADPH/ATP levels and, therefore, keep an active and less ROS-damaged chloroplast electron transport chain. The increased ETR observed in *gl1* and *crr4-3* plants produced NADPH and ATP, not only for carbon assimilation but also for photorespiration and the export of reductants via the malate valve (Yoshida and Noguchi, 2010). The three processes cooccurring in high light provide NAD(P)H to the mETC via sugar oxidation, Gly decarboxylation, and malate oxidation. Under these conditions, both COX and AOX pathways oxidized all the reductant power from the chloroplast, as observed in *gl1* plants after 2 h of HL treatment. Indeed, in a very recent study in Arabidopsis *aox1a* mutants, we showed that the AOX pathway can support photorespiration under HL conditions (Watanabe et al., 2016). However, when the light stress conditions were more severe (indicated by higher levels of photoinhibition), only the COX but not the AOX pathway showed a response to HL stress. Moreover, the impairment of the CEF-PSI in double mutants caused severe damage to the photosynthetic electron transport chain already after 2 h of HL stress, as indicated by the highest levels of chronic photoinhibition. Such severe impairment of the chloroplast ETR probably restricted the generation of chloroplast-derived substrates/reductants by any of the three processes described above and, thus, limited the response of the mETC. Importantly, the statistically significant correlation observed between in vivo respiratory activities and the NADH-NAD^+ ratio supports this view (Fig. 6).

In order to better understand the metabolic links involved in the attenuated respiratory response as a consequence of CEF-PSI impairment under HL stress, metabolite profiles and also their correlation to the respiratory activities in vivo were analyzed (Fig. 6; Supplemental Fig. S4). The induction pattern of sugar levels such as Suc, Gal, and especially Glc was highly correlated to ν_{cyt}, possibly indicating the fueling of respiration by the increase in photosynthesis-derived substrates. In relation to this, pyruvate and tricarboxylic acid cycle intermediates such as succinate, fumarate, and 2-oxoglutarate as well as the 2-oxoglutarate-citrate ratio also showed positive and significant correlations to ν_{cyt}. 2-Oxoglutarate is a key metabolite in nitrogen metabolism, being used as a carbon skeleton for amino acid synthesis (Araújo et al., 2014a). In this study, ν_{cyt} also was positively correlated to several amino acids. Taken together, the correlations observed suggest that ν_{cyt} may oxidize matrix NADH, providing ATP and allowing tricarboxylic acid cycle carbon flow toward amino acid and protein synthesis under severe HL stress. Pro synthesis requires carbon flow from 2-oxoglutarate and Glu as well as ATP (Szabados and Savouré, 2010), and remarkably, it was one of the highest accumulated metabolites following HL treatment in all genotypes. Although not correlated directly to ν_{cyt}, a high synthesis of this ROS-protective metabolite can be speculated, which likely would require a high rate of ATP-coupled respiration. In agreement, significant and positive correlations of ν_{cyt} with Phe also may indicate a high ATP demand for the synthesis of secondary metabolites with an important protective role under HL conditions (Tohge et al., 2013). Also, Tyr was accumulated continuously after HL treatment at very high levels, particularly in double mutants that showed the highest levels after 8 h of HL stress (10-fold increase). Recently, a new alternative pathway was described to link Tyr and Phe metabolism (Yoo et al., 2013), presenting the possibility that Tyr accumulation also contributes to the synthesis of the secondary metabolites derived from Phe (Tohge et al., 2013). In addition, given that Phe is a precursor for UQ biosynthesis (Block et al., 2014; Tohge et al., 2014), correlations to an enhanced ν_{cyt} under HL stress appear to reveal direct metabolic links to the mitochondrial electron transport that warrant further investigation.

Finally, Gly was the metabolite that exhibited the greatest increase following HL treatment, as observed previously in Arabidopsis Col-0 plants after HL treatment (Florez-Sarasa et al., 2012), which suggests a high photorespiratory activity (Timm and Bauwe, 2013). However, this increase was much lower in *pgr5* and, more strikingly, it was almost abolished in the double mutants compared with *gl1* and *crr4-3*. These results denote a link between CEF-PSI and photorespiration. Recently, it was reported that CEF-PSI is increased under photorespiratory and HL conditions, thus indicating the cooperation of both processes as energy-balancing mechanisms under HL conditions (Walker et al., 2014). Photorespiration under HL contributes to the consumption of the excess of reducing power, thus acting as a photoprotective mechanism to avoid photoinhibiton (Takahashi and Badger, 2011). Thus, a high photorespiratory flux, as expected in the HL conditions applied in this study, produced a huge increase in Gly, which is a major substrate for mitochondria in illuminated leaves (Dry et al., 1983; Igamberdiev et al., 1997). In agreement, Gly and the Gly-Ser ratio showed among the highest correlation coefficients with the ν_{cyt}, which suggests that the COX pathway can be involved in the reoxidation of the NADH from Gly decarboxylation. In parallel, ν_{cyt} also was highly and negatively correlated to NADH-NAD^+ ratios and glycerate, which is one of the typical metabolites altered in photorespiratory mutants (Timm and Bauwe, 2013). Interestingly, Sweetlove et al. (2006) found that an uncoupled mitochondrial electron transport by the action of UCP was important to keep the photorespiratory oxidation of Gly to Ser, which in turn benefits photosynthetic performance. Taken together, these observations strongly suggest that the ν_{cyt} permits the oxidation of NADH derived from an HL-stimulated Gly-to-Ser decarboxylation under severe oxidative stress in cooperation with active UCPs. In this way, the ν_{cyt} can

act as a sink for the excess of electrons from the chloroplast via photorespiratory Gly oxidation, thus improving photosynthetic performance and reducing photoinhibition when ν_{alt} is not induced due to severe HL-induced oxidative stress. Notably, ν_{cyt} was more increased in *AOX1a* antisense plants than in the wild type under HL stress, thus compensating for the lack of ν_{alt} increase under HL stress (Florez-Sarasa et al., 2011).

CONCLUSION

The in vivo activities of the mitochondrial COX and AOX pathways were studied, to our knowledge for the first time, in CEF-PSI mutants under growth and HL conditions. In addition, the AOX pathway capacity also was determined and was highly and positively correlated to photoinhibition, probably due to the effect of photosynthesis-derived ROS on the observed induced AOX expression. However, the ν_{alt} was not higher in CEF-PSI mutants than in wild-type (*gl1*) plants under HL conditions, thus partially refuting our hypothesis. The severe metabolic impairment observed in CEF-PSI mutants may underlie the reason for the lack of an AOX activity response (i.e. due to an inactivation by lipid peroxidation products; Winger et al., 2005), which was indeed engaged in the less severely stressed *gl1* plants after 2 h of HL treatment, in agreement with previous results (Florez-Sarasa et al., 2011, 2012) and suggestions (Yoshida et al., 2007). Despite the severity of the HL stress, the ν_{cyt} was induced in all genotypes and was tightly linked to their photosynthetic performance. The correlations with metabolite changes suggest that ν_{cyt} is highly coordinated with stress-related amino acid synthesis. More strikingly, the severely attenuated response of the Gly-Ser ratio in *pgr5* and double mutants suggests an impaired photorespiration that was correlated with an attenuated response of the ν_{cyt}. In addition, NADH-NAD$^+$ ratios were strongly and negatively correlated with ν_{cyt}. We propose that ν_{cyt} can act as a sink for the excess of electrons from the chloroplast via photorespiratory Gly oxidation, thus reducing photoinhibition when ν_{alt} is not induced under severe HL stress. These observations open new perspectives for further studies on the in vivo role and regulation of the mETC in leaves under HL stress. We speculate that such a new in vivo role of the COX pathway can be accomplished partially through an ATP-uncoupled electron transport (i.e. ROS activation of UCPs), although more experiments will be needed to establish the exact mechanism by which this occurs.

MATERIALS AND METHODS

Plant Material and Growth Conditions

Plants of Arabidopsis (*Arabidopsis thaliana*) wild type (ecotype Col-0 *gl1*) and mutants were grown in a growth chamber (Fitotron UIB) under controlled conditions: temperature of 25°C, relative humidity above 40%, 12-h photoperiod, and light intensity of 80 μmol m^{-2} s^{-1} (GL conditions). Plants grown for 4 to 5 weeks under GL were transferred for 2, 4, and 8 h to 800 μmol m^{-2} s^{-1}, considered HL conditions. Arabidopsis *pgr5* is deficient in the Fd-dependent CEF-PSI pathway (Munekage et al., 2002), while *crr4-3* is deficient in the NDH-dependent pathway (Kotera et al., 2005). Also, the double mutant *pgr5 crr4-3* was a gift from Toshiharu Shikanai. The rosettes of the *pgr5* and *crr4-3* single mutants were slightly smaller than those of *gl1* plants after 4 weeks of growth. On the other hand, double mutants presented pale leaves and growth was more affected; therefore, this genotype was grown for 5 weeks in order to reach a similar developmental stage (i.e. number of leaves) to the other three genotypes (Fig. 1).

Chlorophyll Fluorescence

The ΦPSII was obtained from chlorophyll fluorescence measurements in the light by setting the actinic light of a portable pulse amplitude modulation fluorometer (PAM-2000; Walz) to 80 or 800 μmol m^{-2} s^{-1} for GL and HL measurements, respectively. Chloroplast ETR was calculated as the product of ΦPSII × actinic light intensity × 0.84 × 0.5. In addition, qP, qN and NPQ, and F_v/F_m values were obtained from chlorophyll fluorescence measurements in the light and after 30 min of dark adaptation with the PAM-2000 fluorometer. Also, %TPI, %CPI, and %DPI were obtained as described previously by Florez-Sarasa et al. (2011) with a slight modification; in this study, the F_v/F_{mmax} value was obtained from the mean value of F_v/F_{m30} under GL for *gl1* plants (i.e. %CPI in *gl1* plants is 0) in order to compare all the data with *gl1*. Ten to 12 replicates were performed per line and experimental condition.

Respiration Measurements

Measurements of oxygen isotope fractionation during respiration were performed as described by Florez-Sarasa et al. (2007) to determine the activities of the COX and AOX pathways in vivo. The oxygen isotope fractionation of the AOX pathway required for the electron partitioning calculation (Guy et al., 1989) was determined after incubation with 10 mM KCN as described previously (Florez-Sarasa et al., 2007); a mean value of 30.5‰ was used from all the measurements performed in the mutant and wild-type plants because no differences were observed among genotypes (data not shown). On the other hand, an oxygen isotope fractionation of the AOX pathway value of 20.9‰ was taken from previous measurements in Arabidopsis leaves (Florez-Sarasa et al., 2007). Four to five replicates per line and experimental condition were performed.

In addition, the AOX capacity was determined with a Clark-type oxygen electrode as described previously (Florez-Sarasa et al., 2009). Four to 10 replicates per line and experimental condition were performed.

Metabolite Profiling and Pyridine Nucleotide Determinations

Metabolite extractions were performed as described previously (Lisec et al., 2006) using approximately 150 mg of frozen-powdered leaf tissue. Derivatization and gas chromatography-time of flight-mass spectrometry analyses were carried out as described previously (Lisec et al., 2006). Metabolites were identified manually using the TagFinder plug-in of the TagFinder software (Luedemann et al., 2008) and the reference library mass spectra and retention indices housed in the Golm Metabolome Database (http://gmd.mpimp-golm.mpg.de; Kopka et al., 2005). The metabolite ratios were calculated by dividing the signal intensities of the selected masses for the corresponding metabolites, and no calibration was performed with known concentrations of the reference compounds; therefore, the ratios obtained were only used to compare the HL responses among the different genotypes but do not indicate the absolute (actual) ratios. Data were normalized to the mean value of wild-type (*gl1*) plants in GL conditions (i.e. the value of all metabolites and ratios for *gl1* at GL was set to 1). Values presented are means ± SE of six replicates, with each replicate representing a pool of three rosettes.

For pyridine nucleotides, two aliquots of 25 mg each of frozen-powdered leaf tissue (i.e. from the same frozen-powdered material used for GC-MS metabolite analysis) were used to determine the reduced (NADH and NADPH) and the oxidized (NAD$^+$ and NADP$^+$) forms. Extractions and spectrophotometer determinations were performed as described by Kühn et al. (2015).

Western Blotting

Aliquots of 20 mg of frozen-powdered leaf tissue (i.e. from the same frozen-powdered material used for GC-MS metabolite analysis) were used to extract proteins by adding 100 μL of SDS sample buffer (2% [w/v] SDS, 62.5 mM Tris-HCl [pH 6.8], 10% [v/v] glycerol, and 0.007% [w/v] Bromophenol Blue) as well

as 50 mM DTT and a protease inhibitor tablet (Roche). Samples were then incubated for 30 min on ice to allow full reduction of the AOX protein. Thereafter, samples were boiled at 95°C for approximately 5 min and the homogenate was centrifuged at 14,000 rpm for 10 min. The supernatant was transferred into a new tube and kept at −20°C for later analysis. Twenty microliters was loaded and separated on 12% SDS-PAGE gels and transferred to nitrocellulose membranes using the wet Mini-PROTEAN system of Bio-Rad. The following primary antibodies and dilutions were used to detect mitochondrial proteins: monoclonal anti-porin (PM035; from Dr. Tom Elthon) at 1:5,000 dilution; polyclonal anti-AOX (AS04054; Agrisera) at 1:500 dilution; polyclonal anti-COXII (AS04053A; Agrisera) at 1:1,000 dilution; and polyclonal anti-UCP (AS121850; Agrisera) at 1:1,000 dilution. Secondary antibodies linked to horseradish peroxidase were used (Sigma-Aldrich). The signals were detected by chemiluminescence using Pierce ECL Western Blotting Substrate (Thermo Fisher) and a Luminescent Image Analyzer (G-Box-Chemi XT4; Syngene). The protein band quantifications were performed with GeneTools analysis software from the Luminescent Image Analyzer (G-Box-Chemi XT4; Syngene) according to the manufacturer's instructions. The obtained band intensities for AOX, COX, and UCP were corrected for their corresponding porin band intensities and then normalized to the levels of the *gl1* plants under GL (i.e. *gl1* levels for all the proteins are 100%). Two different immunoblot experiments per protein were performed with very similar results (data not shown), and images shown in Figure 4 and Supplemental Figure S2 belong to one of the two membranes obtained. Samples used in each of the two immunoblot experiments were a mixture of aliquots belonging to two biological replicates from the same six biological replicates used for the GC-MS metabolite analyses (i.e. four of the six biological replicates available were used). The percentage values presented in Figure 4 are means of the two immunoblot experiments.

Statistical Analysis

For the statistical analyses in Figures 2 and 3, Table I, and Supplemental Figure S3, a one-way ANOVA with a level of significance of $P < 0.05$ was performed with SPSS for Windows 17.0, and Duncan's posthoc test was used to determine statistically significant differences. Pearson correlations (Fig. 6; Table II) and their significance ($P < 0.05$) between the fold changes in metabolite levels and the fold changes in respiratory or photosynthetic parameters were determined with Microsoft Excel Software 2010. Student's *t* tests were used for the statistical analyses in Supplemental Table S1 in order to compare all genotypes under the different light treatments with *gl1* under GL levels.

Supplemental Data

The following supplemental materials are available.

Supplemental Figure S1. Plots showing all the relationships between photosynthetic and respiratory parameters.

Supplemental Figure S2. Images showing membranes blotted from entire SDS-PAGE gels of the immunodetected mitochondrial proteins AOX, COXII, UCP, and porin in leaf extracts of *gl1*, *crr4-3*, *pgr5*, and *pgr5 crr4-3* plants under GL and after 4 and 8 h of HL treatment.

Supplemental Figure S3. Pyridine nucleotide levels in the wild type (*gl1*) and CEF-PSI mutants.

Supplemental Figure S4. Plots showing the statistically significant ($P < 0.05$) relationships between fold changes in metabolite levels and in vivo respiratory activities in the wild type (*gl1*) and CEF-PSI mutants.

Supplemental Table S1. Metabolite levels in leaves of *gl1*, *crr4-3*, *pgr5*, and *pgr5 crr4-3* plants under GL and after 2, 4, and 8 h of HL treatment.

Supplemental Table S2. Parameters used for peak annotation in GC-MS analysis.

ACKNOWLEDGMENTS

We thank the staff at the Serveis Cientifico-Tecnics of the Universitat de les Illes Balears for help while running these experiments, especially Dr. Biel Martorell for technical help on the isotope ratio mass spectrometer, and Yunuén Avalos Padilla for assistance during the western-blot experiments.

Received July 9, 2016; accepted October 14, 2016; published October 19, 2016.

LITERATURE CITED

Araújo WL, Martins AO, Fernie AR, Tohge T (2014a) 2-Oxoglutarate: linking TCA cycle function with amino acid, glucosinolate, flavonoid, alkaloid, and gibberellin biosynthesis. Front Plant Sci **5:** 552

Araújo WL, Nunes-Nesi A, Fernie AR (2014b) On the role of plant mitochondrial metabolism and its impact on photosynthesis in both optimal and sub-optimal growth conditions. Photosynth Res **119:** 141–156

Atkin OK, Millar AH, Gardeström P, Day DA (2000) Photosynthesis, carbohydrate metabolism and respiration in leaves of higher plants. *In* RC Leegood, TD Sharkey, S von Caemmerer, eds, Photosynthesis: Physiology and Metabolism. Kluwer, Dordrecht, The Netherlands, pp 153–175

Block A, Widhalm JR, Fatihi A, Cahoon RE, Wamboldt Y, Elowsky C, Mackenzie SA, Cahoon EB, Chapple C, Dudareva N, et al (2014) The origin and biosynthesis of the benzenoid moiety of ubiquinone (coenzyme Q) in *Arabidopsis*. Plant Cell **26:** 1938–1948

Dahal K, Martyn GD, Vanlerberghe GC (2015) Improved photosynthetic performance during severe drought in *Nicotiana tabacum* overexpressing a nonenergy conserving respiratory electron sink. New Phytol **208:** 382–395

Dahal K, Wang J, Martyn GD, Rahimy F, Vanlerberghe GC (2014) Mitochondrial alternative oxidase maintains respiration and preserves photosynthetic capacity during moderate drought in *Nicotiana tabacum*. Plant Physiol **166:** 1560–1574

Day DA, Krab K, Lambers H, Moore AL, Siedow JN, Wagner AM, Wiskich JT (1996) The cyanide-resistant oxidase: to inhibit or not to inhibit, that is the question. Plant Physiol **110:** 1–2

Demmig-Adams B, Cohu CM, Muller O, Adams WW III (2012) Modulation of photosynthetic energy conversion efficiency in nature: from seconds to seasons. Photosynth Res **113:** 75–88

Dry IB, Day DA, Wiskich JT (1983) Preferential oxidation of glycine by the respiratory chain of pea leaf mitochondria. FEBS Lett **158:** 154–158

Dutilleul C, Driscoll S, Cornic G, De Paepe R, Foyer CH, Noctor G (2003) Functional mitochondrial complex I is required by tobacco leaves for optimal photosynthetic performance in photorespiratory conditions and during transients. Plant Physiol **131:** 264–275

Flexas J, Bota J, Galmes J, Medrano H, Ribas-Carbo M (2006) Keeping a positive carbon balance under adverse conditions: responses of photosynthesis and respiration to water stress. Physiol Plant **127:** 343–352

Florez-Sarasa I, Araújo WL, Wallström SV, Rasmusson AG, Fernie AR, Ribas-Carbo M (2012) Light-responsive metabolite and transcript levels are maintained following a dark-adaptation period in leaves of *Arabidopsis thaliana*. New Phytol **195:** 136–148

Florez-Sarasa I, Flexas J, Rasmusson AG, Umbach AL, Siedow JN, Ribas-Carbo M (2011) *In vivo* cytochrome and alternative pathway respiration in leaves of *Arabidopsis thaliana* plants with altered alternative oxidase under different light conditions. Plant Cell Environ **34:** 1373–1383

Florez-Sarasa I, Ostaszewska M, Galle A, Flexas J, Rychter AM, Ribas-Carbo M (2009) Changes of alternative oxidase activity, capacity and protein content in leaves of *Cucumis sativus* wild-type and MSC16 mutant grown under different light intensities. Physiol Plant **137:** 419–426

Florez-Sarasa ID, Bouma TJ, Medrano H, Azcon-Bieto J, Ribas-Carbo M (2007) Contribution of the cytochrome and alternative pathways to growth respiration and maintenance respiration in *Arabidopsis thaliana*. Physiol Plant **129:** 143–151

Galle A, Florez-Sarasa I, Thameur A, de Paepe R, Flexas J, Ribas-Carbo M (2010) Effects of drought stress and subsequent rewatering on photosynthetic and respiratory pathways in *Nicotiana sylvestris* wild type and the mitochondrial complex I-deficient CMSII mutant. J Exp Bot **61:** 765–775

Gandin A, Duffes C, Day DA, Cousins AB (2012) The absence of alternative oxidase AOX1A results in altered response of photosynthetic carbon assimilation to increasing CO_2 in *Arabidopsis thaliana*. Plant Cell Physiol **53:** 1627–1637

Gupta KJ, Zabalza A, van Dongen JT (2009) Regulation of respiration when the oxygen availability changes. Physiol Plant **137:** 383–391

Guy RD, Berry JA, Fogel ML, Hoering TC (1989) Differential fractionation of oxygen isotopes by cyanide-resistant and cyanide-sensitive respiration in plants. Planta **177:** 483–491

Hoefnagel MHN, Millar AH, Wiskich JT, Day DA (1995) Cytochrome and alternative respiratory pathways compete for electrons in the presence of pyruvate in soybean mitochondria. Arch Biochem Biophys **318:** 394–400

Igamberdiev AU, Bykova NV, Gardeström P (1997) Involvement of cyanide-resistant and rotenone-insensitive pathways of mitochondrial electron transport during oxidation of glycine in higher plants. FEBS Lett **412:** 265–269

Kopka J, Schauer N, Krueger S, Birkemeyer C, Usadel B, Bergmüller E, Dörmann P, Weckwerth W, Gibon Y, Stitt M, et al (2005) GMD@CSB. DB: the Golm Metabolome Database. Bioinformatics **21:** 1635–1638

Kotera E, Tasaka M, Shikanai T (2005) A pentatricopeptide repeat protein is essential for RNA editing in chloroplasts. Nature **433:** 326–330

Krömer S (1995) Respiration during photosynthesis. Annu Rev Plant Physiol Plant Mol Biol **46:** 45–70

Kühn K, Obata T, Feher K, Bock R, Fernie AR, Meyer EH (2015) Complete mitochondrial Complex I deficiency induces an up-regulation of respiratory fluxes that is abolished by traces of functional Complex I. Plant Physiol **168:** 1537–1549

Li CR, Liang DD, Li J, Duan YB, Li H, Yang YC, Qin RY, Li L, Wei PC, Yang JB (2013) Unravelling mitochondrial retrograde regulation in the abiotic stress induction of rice ALTERNATIVE OXIDASE 1 genes. Plant Cell Environ **36:** 775–788

Lisec J, Schauer N, Kopka J, Willmitzer L, Fernie AR (2006) Gas chromatography mass spectrometry-based metabolite profiling in plants. Nat Protoc **1:** 387–396

Luedemann A, Strassburg K, Erban A, Kopka J (2008) TagFinder for the quantitative analysis of gas chromatography-mass spectrometry (GC-MS)-based metabolite profiling experiments. Bioinformatics **24:** 732–737

Moore AL, Siedow JN (1991) The regulation and nature of the cyanide-resistant alternative oxidase of plant mitochondria. Biochim Biophys Acta **1059:** 121–140

Munekage Y, Hashimoto M, Miyake C, Tomizawa K, Endo T, Tasaka M, Shikanai T (2004) Cyclic electron flow around photosystem I is essential for photosynthesis. Nature **429:** 579–582

Munekage Y, Hojo M, Meurer J, Endo T, Tasaka M, Shikanai T (2002) PGR5 is involved in cyclic electron flow around photosystem I and is essential for photoprotection in Arabidopsis. Cell **110:** 361–371

Nunes-Nesi A, Araújo WL, Fernie AR (2011) Targeting mitochondrial metabolism and machinery as a means to enhance photosynthesis. Plant Physiol **155:** 101–107

Obata T, Florian A, Timm S, Bauwe H, Fernie AR (2016) On the metabolic interactions of (photo)respiration. J Exp Bot **67:** 3003–3014

Oppenheimer DG, Herman PL, Sivakumaran S, Esch J, Marks MD (1991) A myb gene required for leaf trichome differentiation in Arabidopsis is expressed in stipules. Cell **67:** 483–493

Osmond CB (1994) What is photoinhibition? Some insights from comparisons of shade and sun plants. *In* NR Baker, JR Bowyer, eds, Photoinhibition of Photosynthesis: From Molecular Mechanisms to the Field. BIOS Science Publishers, Oxford, pp 1–24

Pintó-Marijuan M, Munné-Bosch S (2014) Photo-oxidative stress markers as a measure of abiotic stress-induced leaf senescence: advantages and limitations. J Exp Bot **65:** 3845–3857

Priault P, Tcherkez G, Cornic G, De Paepe R, Naik R, Ghashghaie J, Streb P (2006) The lack of mitochondrial complex I in a CMSII mutant of *Nicotiana sylvestris* increases photorespiration through an increased internal resistance to CO_2 diffusion. J Exp Bot **57:** 3195–3207

Radwanski ER, Last RL (1995) Tryptophan biosynthesis and metabolism: biochemical and molecular genetics. Plant Cell **7:** 921–934

Raghavendra AS, Padmasree K (2003) Beneficial interactions of mitochondrial metabolism with photosynthetic carbon assimilation. Trends Plant Sci **8:** 546–553

Rasmusson AG, Fernie AR, van Dongen JT (2009) Alternative oxidase: a defence against metabolic fluctuations? Physiol Plant **137:** 371–382

Rasmusson AG, Geisler DA, Møller IM (2008) The multiplicity of dehydrogenases in the electron transport chain of plant mitochondria. Mitochondrion **8:** 47–60

Rhoads DM, Umbach AL, Subbaiah CC, Siedow JN (2006) Mitochondrial reactive oxygen species: contribution to oxidative stress and interorganellar signaling. Plant Physiol **141:** 357–366

Ribas-Carbo M, Berry JA, Yakir D, Giles L, Robinson SA, Lennon AM, Siedow JN (1995) Electron partitioning between the cytochrome and alternative pathways in plant mitochondria. Plant Physiol **109:** 829–837

Ribas-Carbo M, Robinson SA, Giles L (2005) The application of the oxygen-isotope technique to assess respiratory pathway partitioning. *In* H Lambers, M Ribas-Carbo, eds, Plant Respiration: From Cell to Ecosystem. Advances in Photosynthesis and Respiration Series, **Vol 18**. Springer, Dordrecht, The Netherlands, pp 31–42

Scheibe R (2004) Malate valves to balance cellular energy supply. Physiol Plant **120:** 21–26

Shikanai T (2007) Cyclic electron transport around photosystem I: genetic approaches. Annu Rev Plant Biol **58:** 199–217

Steyn WJ, Wand SJE, Holcroft DM, Jacobs G (2002) Anthocyanins in vegetative tissues: a proposed unified function in photoprotection. New Phytol **155:** 349–361

Stiti N, Missihoun TD, Kotchoni SO, Kirch HH, Bartels D (2011) Aldehyde dehydrogenases in *Arabidopsis thaliana*: biochemical requirements, metabolic pathways, and functional analysis. Front Plant Sci **2:** 65

Sweetlove LJ, Lytovchenko A, Morgan M, Nunes-Nesi A, Taylor NL, Baxter CJ, Eickmeier I, Fernie AR (2006) Mitochondrial uncoupling protein is required for efficient photosynthesis. Proc Natl Acad Sci USA **103:** 19587–19592

Szabados L, Savouré A (2010) Proline: a multifunctional amino acid. Trends Plant Sci **15:** 89–97

Takahashi S, Badger MR (2011) Photoprotection in plants: a new light on photosystem II damage. Trends Plant Sci **16:** 53–60

Timm S, Bauwe H (2013) The variety of photorespiratory phenotypes: employing the current status for future research directions on photorespiration. Plant Biol (Stuttg) **15:** 737–747

Tohge T, Obata T, Fernie AR (2014) Biosynthesis of the essential respiratory cofactor ubiquinone from phenylalanine in plants. Mol Plant **7:** 1403–1405

Tohge T, Watanabe M, Hoefgen R, Fernie AR (2013) Shikimate and phenylalanine biosynthesis in the green lineage. Front Plant Sci **4:** 62

Van Aken O, Giraud E, Clifton R, Whelan J (2009) Alternative oxidase: a target and regulator of stress responses. Physiol Plant **137:** 354–361

Vanlerberghe GC (2013) Alternative oxidase: a mitochondrial respiratory pathway to maintain metabolic and signaling homeostasis during abiotic and biotic stress in plants. Int J Mol Sci **14:** 6805–6847

Vercesi AE, Borecký J, Maia IdeG, Arruda P, Cuccovia IM, Chaimovich H (2006) Plant uncoupling mitochondrial proteins. Annu Rev Plant Biol **57:** 383–404

Vidal G, Ribas-Carbo M, Garmier M, Dubertret G, Rasmusson AG, Mathieu C, Foyer CH, De Paepe R (2007) Lack of respiratory chain complex I impairs alternative oxidase engagement and modulates redox signaling during elicitor-induced cell death in tobacco. Plant Cell **19:** 640–655

Walker BJ, Strand DD, Kramer DM, Cousins AB (2014) The response of cyclic electron flow around photosystem I to changes in photorespiration and nitrate assimilation. Plant Physiol **165:** 453–462

Watanabe CK, Hachiya T, Takahara K, Kawai-Yamada M, Uchimiya H, Uesono Y, Terashima I, Noguchi K (2010) Effects of AOX1a deficiency on plant growth, gene expression of respiratory components and metabolic profile under low-nitrogen stress in *Arabidopsis thaliana*. Plant Cell Physiol **51:** 810–822

Watanabe CK, Yamori W, Takahashi S, Terashima I, Noguchi K (2016) Mitochondrial alternative pathway-associated photoprotection of photosystem II is related to the photorespiratory pathway. Plant Cell Physiol **57:** 1426–1431

Winger AM, Millar AH, Day DA (2005) Sensitivity of plant mitochondrial terminal oxidases to the lipid peroxidation product 4-hydroxy-2-nonenal (HNE). Biochem J **387:** 865–870

Yamamoto H, Peng L, Fukao Y, Shikanai T (2011) An Src homology 3 domain-like fold protein forms a ferredoxin binding site for the chloroplast NADH dehydrogenase-like complex in *Arabidopsis*. Plant Cell **23:** 1480–1493

Yoo H, Widhalm JR, Qian Y, Maeda H, Cooper BR, Jannasch AS, Gonda I, Lewinsohn E, Rhodes D, Dudareva N (2013) An alternative pathway contributes to phenylalanine biosynthesis in plants via a cytosolic tyrosine:phenylpyruvate aminotransferase. Nat Commun **4:** 2833

Yoshida K, Noguchi K (2010) Interaction between chloroplasts and mitochondria: activity, function, and regulation of the mitochondrial respiratory system during photosynthesis. *In* F Kempken, ed, Plant Mitochondria. Springer, New York, pp 383–409

Yoshida K, Terashima I, Noguchi K (2007) Up-regulation of mitochondrial alternative oxidase concomitant with chloroplast over-reduction by excess light. Plant Cell Physiol **48:** 606–614

Yoshida K, Watanabe C, Kato Y, Sakamoto W, Noguchi K (2008) Influence of chloroplastic photo-oxidative stress on mitochondrial alternative oxidase capacity and respiratory properties: a case study with Arabidopsis yellow variegated 2. Plant Cell Physiol **49:** 592–603

Yoshida K, Watanabe CK, Terashima I, Noguchi K (2011) Physiological impact of mitochondrial alternative oxidase on photosynthesis and growth in *Arabidopsis thaliana*. Plant Cell Environ **34:** 1890–1899

Zhao Y (2012) Auxin biosynthesis: a simple two-step pathway converts tryptophan to indole-3-acetic acid in plants. Mol Plant **5:** 334–338